

(HUANJING KEXUE)

# ENVIRONMENTAL SCIENCE

第39卷 第3期

Vol.39 No.3

2018

\_\_\_\_ 中国科学院生态环境研究中心 主办

斜学出版社出版



## 环龙科豆 (HUANJING KEXUE)

## ENVIRONMENTAL SCIENCE

第39 卷 第3 期 2018年3月15日

## 次

## 铜铁氧体法处理模拟染料废水

韩志勇1,韩昆1,郝昊天2,3,于建伟2,4,石宝友2,4\*,庄媛2,孔岩1

(1. 兰州理工大学石油化工学院, 兰州 730050; 2. 中国科学院生态环境研究中心, 中国科学院饮用水科学与技术重点实验室, 北京 100085; 3. 北京林业大学环境科学与工程学院, 北京 100083; 4. 中国科学院大学, 北京 100049)

摘要: 探讨了不同反应条件对铜铁氧体法(*in situ* copper ferrite process)处理亚甲基蓝、结晶紫、刚果红和酒石黄这 4 种不同模拟染料废水的效果,并以亚甲基蓝模拟染料废水为例,研究了铁氧体法处理染料废水的反应热力学和生成沉淀物的物理化学性质,提出了铜铁氧体法处理模拟染料废水的主要机制. 结果表明,通过调节铜铁氧体法的反应条件对 4 种模拟染料废水均可取得良好的处理效果. 在  $c(Cu^{2+})=0.01 \text{ mol} \cdot L^{-1}$ ,  $c(Fe^{2+})=0.025 \text{ mol} \cdot L^{-1}$ , c(OH)/c(M)=1.7(投加的氢氧根离子与金属的摩尔比),T=40  $\mathbb{C}$ ,t=60 min 的条件下,铜铁氧体法对亚甲基蓝、酒石黄、结晶紫、刚果红这 4 种模拟染料废水的最大处理能力分别达到 349. 2、382. 2、402. 5、831. 8 mg·g  $^{-1}$ . 铜铁氧体法处理模拟染料废水的机制主要是高活性的新生态Fe-Cu 沉淀物对染料分子的高效吸附和在沉淀物聚集过程中的卷扫、包裹作用. 沉淀物通过磁分离、分解提纯、高温煅烧可生成铜铁氧体晶体材料回收利用.

关键词:铜铁氧体法;模拟染料废水;吸附;磁分离;回收利用

中图分类号: X703.1 文献标识码: A 文章编号: 0250-3301(2018)03-1195-07 **DOI**: 10.13227/j. hjkx. 201706099

## Treating Simulated Dye Wastewater by an In Situ Copper Ferrite Process

HAN Zhi-yong<sup>1</sup>, HAN Kun<sup>1</sup>, HAO Hao-tian<sup>2,3</sup>, YU Jian-wei<sup>2,4</sup>, SHI Bao-you<sup>2,4</sup>\*, ZHUANG Yuan<sup>2</sup>, KONG Yan<sup>1</sup>

(1. College of Petrochemical Engineering, Lanzhou University of Technology, Lanzhou 730050, China; 2. Key Laboratory of Drinking Water Science and Technology, Research Center for Eco-Environmental Sciences, Chinese Academy of Sciences, Beijing 100085, China; 3. College of Environmental Science and Engineering, Beijing Forestry University, Beijing 100083, China; 4. University of Chinese Academy of Sciences, Beijing 100049, China)

**Abstract:** Four types of simulated dye wastewater containing methylene blue, tartrazine, Congo red, and crystal violet were treated by an *in situ* copper ferrite process, and the influencing factors of the operational parameters in this process were studied. The main mechanism of dye removal was suggested by reaction thermodynamics and solid products characterization for methylene blue removal. The results showed that an *in situ* copper ferrite process could effectively remove four kinds of simulated dyes by adjusting reaction conditions appropriately. The maximum capacities of the *in situ* copper ferrite process for methylene blue, crystal violet, tartrazine, and Congo red were 349.2, 382.2, 402.5 and 831.8 mg·g<sup>-1</sup>, respectively, under reaction condition of c ( $Cu^{2+}$ ) of 0.01 mol·L<sup>-1</sup>, c ( $Fe^{2+}$ ) of 0.025 mol·L<sup>-1</sup>, c ( $Fe^{2+}$ ) of 0.025 mol·L<sup>-1</sup>, e ( $Fe^{2+$ 

Key words: in situ copper ferrite process; simulated dyes wastewater; adsorption; magnetic separation; recycling

全世界每年大约生产8×10<sup>5</sup> t 的染料,这些染料被广泛应用于食品、纺织、印染、皮革制造等行业<sup>[1]</sup>.在整个染料生产过程中流失的染料占了全部染料产量的15%<sup>[2]</sup>.染料废水具有水量大、有机物含量高、色度高、"三致"毒性等特点,如果处理不当,会给生态环境和人体健康带来严重威胁<sup>[3]</sup>.常见的染料废水处理方法主要包括吸附法、混凝-絮凝法、生物法、膜分离法等<sup>[4,5]</sup>,其中吸附技术因为其易于操作,成本低和效率高等特点,被广泛应用于处理染料废水.吸附剂的比表面积较低、分离回收困难成为

当前吸附法高效处理染料废水的瓶颈[6,7].

铁氧体法(ferrite process)是利用非铁元素与铁元素之间的共沉淀作用生成铁氧体,去除废水中重金属和部分有机污染物、泥沙、微生物及其他可溶性无机盐的一种方法<sup>[8,9]</sup>.研究表明,新生态的氧化物往往具有更大的比表面积和更好的吸附性

收稿日期: 2017-06-11; 修订日期: 2017-08-29

基金项目: 国家重点研发计划项目(2016YFA0203204)

作者简介: 韩志勇(1976~), 男, 博士, 副教授, 主要研究方向为水资源利用与水污染控制, E-mail; hanzhy\_009@ sina.

\* 通信作者, E-mail: byshi@ rcees. ac. cn

能<sup>[10,11]</sup>. 若采用铁氧体法处理染料废水,在新生态铁氧体材料生成的同时,很可能实现对染料的有效去除,同时铁氧体自身的磁性会使固液分离更加简捷. 目前这种处理染料废水的方法尚未有文献报道. 因此,本文拟采用铜铁氧体法处理模拟染料废水,重点考察不同反应条件对铜铁氧体法处理效果的影响,建立反应动力学和热力学模型,结合固相产物表征等手段对相关机制进行探讨,并对该法分离回收铜铁氧体的可行性做了初步分析.

## 1 材料与方法

#### 1.1 实验试剂

依据染料的阴、阳离子类型及分子体积选取了亚甲基蓝、结晶紫、刚果红、酒石黄这 4 种常用染料,染料主要特征参数见表 1. 其中 4 种染料的分子体积使用 Chem-Bio3D 软件中的 MM2 力场参数进行模拟计算 [12],最大吸收波长 ( $\lambda_{max}$ )由 UV-6100型紫外分光光度计测得.

七水合硫酸亚铁( $FeSO_4 \cdot 7H_2O$ )、五水合硫酸铜( $CuSO_4 \cdot 5H_2O$ )、氢氧化钠(NaOH)、亚甲基蓝(三水)、结晶紫、刚果红、酒石黄均为分析纯,购于国药集团化学试剂有限公司,所有用水均为去离子水.

## 1.2 实验方法

取 80 mL 浓度为 200 mg·L<sup>-1</sup>的染料储备液于  $30 \times 300 \, (\text{mm})$  的试管,以 320 mL·min<sup>-1</sup>的流量持续曝气,水浴加热控制反应温度(T). 向试管中投加一定量的  $\text{CuSO}_4 \cdot 5\text{H}_2\text{O}$  和  $\text{FeSO}_4 \cdot 7\text{H}_2\text{O}$  调节溶液中  $\text{Fe}^{2+}$ 与  $\text{Cu}^{2+}$ 的浓度比值 c(Fe)/c(Cu),混合均匀后向试管中缓慢滴加 NaOH 溶液,改变投加的氢氧根离子与总的金属( $\text{Fe}^{2+}$  和  $\text{Cu}^{2+}$ )浓度的比值 c(OH)/c(M),每组实验均设置空白样. 按不同时间 t 取样,经 0. 45  $\mu$ m 膜过滤后,使用紫外分光光度计测定剩余染料浓度,并使用日本岛津公司的ICPE-9800 型电感耦合等离子光谱仪(ICP-OES)测定溶液中剩余总铜、总铁浓度.

表 1 染料的物理化学特征

	Table 1	Physicochemical	characteristics	of	the	studied	dves	
--	---------	-----------------	-----------------	----	-----	---------	------	--

	/ #	1 / #	1	
染料类型	染料名称	分子体积/nm³	相对分子质量	$\lambda_{ m max}/{ m nm}$
阳离子	亚甲基蓝 /	0.278	319. 86	664
	结晶紫	0. 392	407. 99	584
阴离子	酒石黄	0. 327	534. 36	426
	刚果红	0.429	696. 68	498

## 1.3 沉淀物的表征

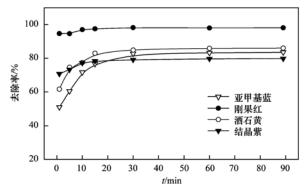
使用德国蔡司公司的 Merlin 型场发射电子扫描显微镜(SEM)观察沉淀物的表观形貌变化,使用日本岛津公司的 ASAP2020HD88 型全自动比表面积及微孔物理吸附仪测定沉淀物的比表面积,使用英国马尔文公司的 Master sizer 2000 型纳米粒度及Zeta 电位分析仪测定沉淀物的粒径变化,使用德国布鲁克公司的 VERTEX 70 型红外光谱仪(FT-IR)表征沉淀物的官能团变化,使用日本岛津公司的X'Pert PRO MPD 型 X 射线粉末衍射仪(XRD)表征沉淀物的晶型结构.

#### 2 结果与讨论

## 2.1 反应时间的影响及吸附动力学研究

反应时间对铜铁氧体法处理 4 种模拟染料废水的影响见图 1. 刚果红的去除率在 1 min 时就已经达到了 90% 以上;对其它 3 种染料,0~30 min 是染料去除的主要阶段,30 min 以后染料去除率变化不大.此外,反应时间决定溶液中 Fe 的价态变化,

Fe<sup>3+</sup>越多生成材料的磁性越好<sup>[13]</sup>. 有报道指出,为了达到良好的磁分离性能反应时间应控制在 40 min以上<sup>[14]</sup>,本文后续研究选定的反应时间为 60 min.



 $c(\,\mathrm{Cu^{2\,+}}\,) = 0.\,\,01\,\,\mathrm{mol}\cdot\mathrm{L^{-1}}\,,\,\,c(\,\mathrm{Fe^{2\,+}}\,) = 0.\,\,025\,\,\mathrm{mol}\cdot\mathrm{L^{-1}}\,,$   $c(\,\mathrm{OH})/c(\,\mathrm{M}) = 1.\,7\,,\,\,T = 40\,\,^{\circ}\!\mathrm{C}$ 

### 图 1 反应时间对染料去除率的影响

Fig. 1 Effects of reaction time on dye removal efficiency

为了进一步了解反应动力学特性,借用吸附动力学的数据处理方式,采用准一级动力学模型和准二级动力学模型对铜铁氧体法去除染料的数据进行

了拟合, 拟合结果见表 2. 其中:

$$q_t = \frac{\left(c_0 - c_t\right)V}{m}$$

式中,  $q_i$  为吸附平衡时的吸附量( $mg \cdot g^{-1}$ );  $c_0 \cdot c_i$  分别为反应前后染料浓度( $mg \cdot L^{-1}$ ); V 为溶液体积(L); m 为投加进溶液中的  $Cu^{2+}$  与  $Fe^{2+}$  的质量和(g).

准一级动力学模型和准二级动力学模型的表达 式分别为<sup>[15]</sup>:

$$\lg(q_e - q_t) = \lg q_e - k_1 t$$

$$\frac{t}{q_t} = \frac{1}{k_2 q_e^2} + \frac{t}{q_e}$$

式中,  $k_1(\min^{-1})$ 、 $k_2[g\cdot(\operatorname{mg}\cdot\operatorname{min})^{-1}]$ 分别是准一级动力学、准二级动力学的吸附速率常数;  $q_e(\operatorname{mg}\cdot\operatorname{g}^{-1})$ 和 $q_i(\operatorname{mg}\cdot\operatorname{g}^{-1})$ 分别为平衡吸附容量和在 $t(\operatorname{min})$ 时间的吸附量.

根据表中拟合相关系数 R<sup>2</sup> 可知, 准二级动力学方程比准一级动力学方程能更好地拟合铜铁氧体法处理 4 种模拟染料废水的行为, 计算出的平衡吸附容量也更接近实验数据. 该反应在一定程度上符合准二级动力学模型, 但准二级动力学方程的拟合相关系数 R<sup>2</sup> 均小于 0.9, 准二级动力学模型不能准确、全部地描述反应过程, 说明该反应可能不是一个单纯的吸附过程.

表 2 铜铁氧体法处理 4 种染料的动力学吸附常数

Table 2 Kinetic parameters for the removal of four dyes by the copper ferrite process

					, , , , , , , , , , , , , , , , , , , ,		
染料种类	实际测定	准	主一级反应动力学	ż		准二级反应动力学	
条件件失	$q_{ m e}/{ m mg}\cdot{ m g}^{-1}$	$q_{ m e}/{ m mg}\cdot{ m g}^{-1}$	$k_1/{ m min}^{-1}$	$R^2$	$q_{ m e}/{ m mg}\cdot{ m g}^{-1}$	$k_2/g \cdot (\text{mg} \cdot \text{min})^{-1}$	$R^2$
亚甲基蓝	81. 86	75. 02	1. 057	0. 495 1	79. 49	$1.647 \times 10^{-2}$	0. 785 5
结晶紫	78. 18	76. 34	2. 385	0. 507 5	77. 16	1. $024 \times 10^{-1}$	0.7297
刚果红	95. 34	94. 12	3. 179	0. 495 6	94. 51	$1.093 \times 10^{-3}$	0. 699
酒石黄	84. 31	80. 44	1. 382	0. 704 8	82. 99	2. $927 \times 10^{-2}$	0.898

### 2.2 Fe/Cu 的影响

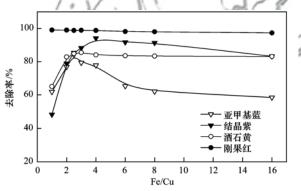
Fe/Cu 浓度比对铜铁氧体法处理 4 种模拟染料废水的影响见图 2. 随着 Fe/Cu 的增大,铜铁氧体法对亚甲基蓝、酒石黄、结晶紫去除率在 Fe/Cu 为 2.5、3、4 处依次出现最大值,随后 3 种染料的去除率均开始下降,其中亚甲基蓝的去除率较酒石黄和结晶紫的去除率下降更加明显,而刚果红的去除率始终变化不大. 结合表 1 发现,去除率最大值的出现顺序与染料的分子体积由小到大的顺序一致,表明 Fe/Cu 的增大可能有利于去除分子体积较大的污染物.铜铁氧体的反应方程式为:

$$x$$
Cu<sup>2+</sup> + (3 -  $x$ ) Fe<sup>2+</sup> + 6 OH<sup>-</sup> + 1/2 O<sub>2</sub>  $\longrightarrow$  Cu<sub>x</sub>Fe<sub>(3-x)</sub>O<sub>4</sub> + 3 H<sub>2</sub>O

根据反应方程式,Fe/Cu 的变化可能产生不同类型的  $Cu_x$ Fe $_{(3-x)}O_4$  及各种复杂的副产物 $^{[16]}$ ,Fe<sup>2+</sup>的增多可能会导致反应过程中更多铁氧化物的迅速生成,从而干扰该沉淀物晶体的生长,造成产物组成的变化,进而影响该过程中新生态氧化物的物理化学性质,最终表现为对不同目标染料分子去除效果的差异. 从经济的角度看,在保证染料高去除率条件下,适当减少  $Cu^{2+}$ 的投加量可以节约成本.

## 2.3 OH/M 的影响

OH/M 浓度比对铜铁氧体法处理 4 种模拟染料 废水的影响及溶液中总铜、总铁剩余浓度的变化分



M = 0.035 mol·L<sup>-1</sup>, OH/M = 1.7, T = 40°C, t = 60 min 图 2 Fe/Cu 对染料去除率的影响

Fig. 2 Effects of Fe/Cu on dye removal efficiency

别见图 3 和表 3. OH/M > 1.7 时, 亚甲基蓝的去除率下降明显. 当 OH/M > 2.1 时, 酒石黄和刚果红去除率开始轻微下降, 而结晶紫去除率变化不大. 这表明不同的污染物所需的碱的投加量有所差异, 分子体积大的污染物所需的 OH/M 相对更高. 而在 OH/M 过高时会导致部分染料的去除率下降, 这可能是因为过多的 OH<sup>-</sup>导致产生 Fe(OH)<sub>2</sub>、Cu(OH)<sub>2</sub> 凝胶<sup>[8]</sup>,使新生态沉淀物的组成和物化性质发生变化,影响染料的去除率. 只投加碱而不投加金属离子的空白实验还发现, 4 种染料中, 刚果红在碱性条件下未发生自沉淀, 其余 3 种染料在高 pH 值下都会发生不同程度的自沉淀. 因此, 结晶紫在 OH/M > 2.1

时去除率上升除了沉淀物结构组成变化以外,结晶 紫自沉淀可能也发挥了一定的作用.

如表 3 所示,OH/M 为 1.7 时,溶液中总铜的剩余浓度仍高达 147 mg·L<sup>-1</sup>远远高出了污水综合排放标准(GB 8978-1996)中 0.5 mg·L<sup>-1</sup>的标准值,造成了重金属污染和资源浪费;在 OH/M 为 2.1 时,溶液中总铜的剩余浓度低于 0.5 mg·L<sup>-1</sup>且总铁的剩余浓度已低于检出限.考虑到 OH/M > 2.1 时铜铁氧体法处理亚甲基蓝的效果大大降低,同时也使结晶紫自沉淀,故在后续的实验中将 OH/M 设为 1.7. 实际应用中应从污染物去除效果和残余金属浓度两个方面合理确定 OH/M 比.

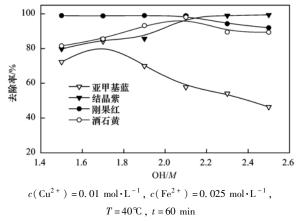


图 3 OH/M 对染料去除率的影响

Fig. 3 Effects of OH/M on dye removal efficiency

表 3 OH/M 比对溶液中总铜、总铁剩余浓度的影响 $^{1)}/mg\cdot L^{-1}$ 

Table 3 Effects of OH/M ratio on residual iron ions and cupric ion concentration/mg·L<sup>-1</sup>

					· · · · · · · · · · · · · · · · · · ·			
OH/M		总铜剩	余浓度			总铁乘	余浓度	
OH/M	亚甲基蓝	结晶紫	刚果红	酒石黄	亚甲基蓝	结晶紫	刚果红	酒石黄
1.5	265	407	429	399	20. 4	87	30. 1	59. 5
1.7	147	330	348	236	0. 028 6	0. 173	0. 017 3	0. 129
1.9	44. 1	77. 3	31.6	16. 7	0. 161	0. 286	0. 081	0. 371
2. 1	0. 129	0.0821	0. 138	0.493	- 1	<i>⇒</i> + .\	_	-/-
2. 3	0.0463	0.0476	0. 118	0. 136	- / 5	+ "/	_	183
2.5	_	_	_	_	- / 0	' + II I	- /	//- } [

1)"—"为检测值低于 ICP-OES 检出限

## 2.4 温度的影响

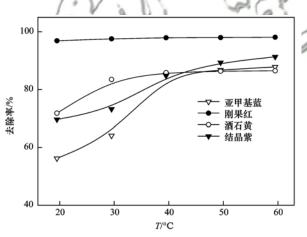
温度对铜铁氧体法处理 4 种模拟染料废水的影响见图 4. 随着温度的上升, 4 种染料的去除率均有不同程度的升高, 其中温度变化对刚果红去除率的影响很小. 温度适当的升高使得溶液中的分子热运动加剧, 加速了反应过程, 同时温度升高也影响新生态铁氧体材料的存在状态, 使其与染料的活性接触位点增多, 更易于染料的去除<sup>[17]</sup>. 采用铜铁氧体法处理染料废水所需温度控制在 40 ~60℃即可,相对于 Tu 等<sup>[14]</sup>采用铁氧体工艺去除 Cu²+ 所需 70 ~90℃的温度条件更为温和, 能耗更低.

## 2.5 吸附等温线

采用 Langmuir 和 Freundlich 模型对铜铁氧体法 去除染料的数据进行拟合, Langmuir 模型用于描述 均质吸附, Freundlich 模型用于描述非均质吸附, 表达式分别为<sup>[18]</sup>:

$$q_e = \frac{K_L q_m c_e}{1 + K_L c_e}$$
$$q_e = K_F c_e^{\frac{1}{n}}$$

式中,  $c_e$  为平衡时染料剩余浓度( $mg \cdot L^{-1}$ );  $K_L$  和  $q_m$  分别是 Langmuir 吸附平衡常数和最大吸附量( $mg \cdot g^{-1}$ );  $K_F$  和 n 是 Freundlich 常数,分别代表吸附剂的吸附能力和吸附强度.



 $c(Cu^{2+}) = 0.01 \text{ mol} \cdot L^{-1}, c(Fe^{2+}) = 0.025 \text{ mol} \cdot L^{-1},$ OH/M = 1.7, t = 60 min

#### 图 4 温度对染料去除率的影响

Fig. 4 Effects of temperature on dye removal efficiency

拟合结果见表 4,结晶紫和酒石黄的吸附等温线更符合 Langmuir 模型,亚甲基蓝和刚果红的吸附等温线更符合 Freundlich 模型.根据 Langmuir 模型拟合的铜铁氧体法处理模拟染料废水的最大处理能力按从小到大的顺序为:亚甲基蓝(349.2 mg·g<sup>-1</sup>) <酒石黄(382.2 mg·g<sup>-1</sup>) <结晶紫(402.5 mg·g<sup>-1</sup>) <刚果红(831.8 mg·g<sup>-1</sup>),这与染料分子体积从小到大的顺序相吻合.铜铁氧体法能对阴阳离子染料都有很好的去除能力,因此静电作用在反应过程中

可能不是主导作用力.

Freundlich 模型拟合铜铁氧体法处理刚果红的 n < 1,属于非优惠吸附,但分析  $2.1 \sim 2.4$  节的数据 发现,改变反应条件刚果红的去除率一直都很高.刚果红是一种金属络合型染料,在反应过程中容易

与  $Fe^{2+}$ 、 $Cu^{2+}$ 形成  $\pi-\pi$  键络合吸附<sup>[19,20]</sup>. 通过对比实验发现,刚果红与  $Fe^{2+}$ 、 $Cu^{2+}$ 均会迅速络合生成沉淀,而其它 3 种染料未出现此现象. 这就合理解释了该法处理刚果红虽属非优惠吸附,但从速率和处理容量方面都是最佳的现象.

表 4 铜铁氧体法处理 4 种染料的等温吸附常数

Table 4	Isothermal	constants	for	tha	four	duce	in	tha	conner	farrita	process	
rabie 4	isomermai	constants	TOL	une	TOUL	uves	Ш	une	copper	territe	Drocess	

染料种类		Langmuir 模型			Freundlich 模型	
采件件矢	$q_{\mathrm{m}}/\mathrm{mg}\cdot\mathrm{g}^{-1}$	$K_{\rm L}/{ m L} \cdot { m mg}^{-1}$	$R^2$	1/n	$K_{\mathrm{F}}/\mathrm{mg} \cdot \mathrm{g}^{-1} (\mathrm{mg} \cdot \mathrm{L}^{-1})^{1/n}$	$R^2$
亚甲基蓝	349. 2	$1.556 \times 10^{-2}$	0. 986 7	0. 444 7	17. 34	0. 999 7
结晶紫	402. 5	$7.32 \times 10^{-3}$	0. 990 9	0. 621 6	12. 09	0. 948 5
刚果红	831. 8	$2.067 \times 10^{-2}$	0. 994 7	1.4115	25. 44	0. 997 5
酒石黄	382. 2	$5.290 \times 10^{-3}$	0. 999 8	0. 621 2	10. 53	0. 972 8

### 2.6 机制探讨

以亚甲基蓝为例,通过反应热力学分析及对沉 淀物的物理化学性质表征,推断染料去除主要机制.

### 2.6.1 吸附热力学

热力学参数包括标准吉布斯自由能变( $\Delta G^{\theta}$ )、标准焓变( $\Delta H^{\theta}$ )和标准熵变( $\Delta S^{\theta}$ ). 热力学方程式如下<sup>[21]</sup>:

$$\ln K_{\rm C} = -\frac{\Delta G^{\theta}}{RT} = \frac{\Delta S^{\theta}}{R} - \frac{\Delta H^{\theta}}{RT}$$
$$K_{\rm C} = \frac{c_{\rm ae}}{c_{\rm e}}$$

式中,  $K_c$  为分配系数;  $c_e$  和  $c_{ae}$  分别为平衡时液相

和固相中的染料浓度 $(mg \cdot L^{-1})$ ; R 为理想气体常数,  $8.314 \ J \cdot (mol \cdot K)^{-1}$ .

根据  $K_c$  的值计算出  $\Delta G^{\theta}$ ,用  $\ln K_c$  值对  $T^{-1}$ 作图,可得到  $\Delta H^{\theta}$  和  $\Delta S^{\theta}$  的值,结果如表 5 所示.  $\Delta G^{\theta}$  始终为负值并处于  $0 \sim -20 \text{ kJ} \cdot \text{mol}^{-1}$ 之间,可认为该反应是一个自发进行的物理吸附过程<sup>[22]</sup>,随着温度的升高  $\Delta G^{\theta}$  数值变大,说明高温下反应更容易进行.  $\Delta H^{\theta}$  为正值,说明该反应过程是吸热反应<sup>[23]</sup>,温度升高有利于反应的进行,这与之前温度影响结果相符合.  $\Delta S^{\theta}$  为正值,表明铜铁氧体法处理亚甲基蓝废水是一个熵增的过程,反应过程中固液界面吸附的随机性增强<sup>[17]</sup>.

表 5 铜铁氧体法处理亚甲基蓝的热力学参数

Table 5 Thermodynamic constants for methylene blue in the copper ferrite process

温度/K	$\Delta G^{ heta}/\mathrm{kJ}\cdot\mathrm{mol}^{-1}$	$\Delta S^{\theta}/\mathrm{kJ}\cdot(\mathrm{mol}\cdot\mathrm{K})^{-1}$	$\Delta H^{\theta}/\mathrm{kJ \cdot mol^{-1}}$	$R^2$
293	-0.6102	0.1366	39. 29	0.9343
303	-1.798	0.1366	39. 29	0.9343
313	-4.159	0.1366	39. 29	0.9343
323	-5.048	0.1366	39. 29	0.9343
333	-5.741	0.1366	39. 29	0.9343

#### 2.6.2 沉淀物的物理化学性质

将铜铁氧体法在去离子水中生成的沉淀物与在亚甲基蓝中得到的沉淀物分别进行清洗、冷冻干燥,其 FT-IR 图谱如图 5(a)所示. 其红外图谱基本一致,这表明反应过程中没有新的化学键的生成,是一个单纯的物理过程,与热力学分析中的结论相一致.

不同时间沉淀物的粒径分析结果如图 5(b)所示.可以看出,粒径随着反应时间不断变大,并且粒径变化的速率与图 2 中亚甲基蓝去除率的变化速率一致,由此推断沉淀物生长的过程应该是染料去除的主要阶段,在这个过程中新生态氧化物逐渐生长,宏观粒径逐渐变大,染料被吸附、卷扫、包裹

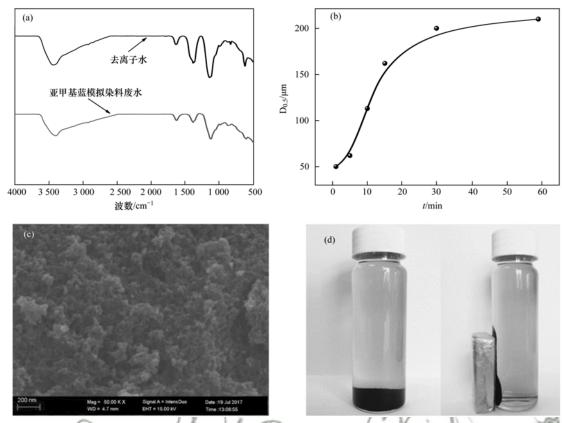
进入新生成的沉淀物中.

30 min 时的沉淀物经分离、冷冻干燥后在扫描电子显微镜下的观察图像如图 5(c)所示. 沉淀物是一个多层多孔的结构,此外,测得 30 min 时沉淀物的比表面积为  $228.7 \text{ m}^2 \cdot \text{g}^{-1}$ . 沉淀物多层多孔的结构以及较大的比表面积有效地提高了传质速率,易于染料的去除.

图 5(d)为该法处理亚甲基蓝后沉淀物的磁分离效果. 在外置磁铁的作用下沉淀物能迅速聚集,证实沉淀物具有良好的磁性.

## 2.7 沉淀物的回收利用

已有研究表明,金属氧化物(CuFe<sub>2</sub>O<sub>4</sub>等)活化 过硫酸盐(或过一硫酸盐)产生的 SO<sub>4</sub>-可有效地氧



(a) 沉淀物的 FT-IR 图谱,(b) 沉淀物粒径随时间变化,(c) 沉淀物的扫描电镜,(d) 沉淀物磁分离效果

## 图 5 沉淀物的物理化学性质

Fig. 5 Physicochemical characteristics of the precipitates

化降解有机污染物<sup>[24~26]</sup>. 向分离的沉淀物中,先加入一定浓度过硫酸钾溶液降解沉淀物中的染料,再将沉淀物在 650% 下煅烧 3~h,采用 XRD 分析煅烧前后的变化,并与在去离子水中制备的沉淀物进行对比,结果如图 6~h 所示. 回收的沉淀物经过煅烧晶体结构更加明显,其主要成分为  $CuFe_2O_4$ ,还有少量的  $Fe_2O_3$ . 与去离子水制备的沉淀物对比发现,

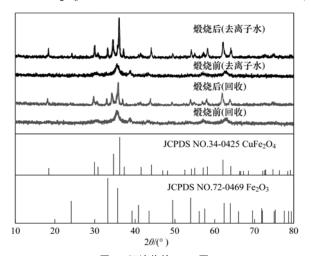


Fig. 6 XRD patterns of the precipitates

图 6 沉淀物的 XRD 图

两者煅烧前后的谱图基本一致. 回收的材料可作为 磁分离技术中的磁种或高级氧化技术中的催化剂, 可实现资源的回收利用.

#### 3 结论

- (1)铜铁氧体法能有效处理多种类型的模拟染料废水,可在60 min 内达到80%以上的去除率. 其对亚甲基蓝、酒石黄、结晶紫、刚果红4种模拟染料废水的处理能力分别达到349.2、382.2、402.5、831.8 mg·g<sup>-1</sup>,处理能力与染料分子的带电性质无关,而与分子体积大小相关.
- (2)铜铁氧体法处理刚果红主要是依靠染料与Fe<sup>2+</sup>、Cu<sup>2+</sup>间的络合作用;处理其他3种染料的过程主要依靠物理作用,在铜铁氧体的生成过程中染料分子被吸附、卷扫和包裹进入新生态Fe—Cu氧化物中.
- (3)铜铁氧体法处理模拟染料废水后的沉淀物进行磁分离、有机物降解纯化、高温煅烧得到CuFe<sub>2</sub>O<sub>4</sub>,可作为磁分离技术中的磁种或污染物降解催化剂,顺应了废水处理绿色分离、资源回收的发展方向.

#### 参考文献:

2572.

[1] Lin J Y, Ye W Y, Zeng H M, et al. Fractionation of direct dyes and salts in aqueous solution using loose nanofiltration membranes
 [J]. Journal of Membrane Science, 2015, 477: 183-193.

[2] 常自强, 陈复彬, 张玉, 等. 刚果红分子印迹聚合物纳米微

- 球的合成及吸附性能[J]. 环境科学, 2015, **36**(7): 2564-2572.

  Chang Z Q, Chen F B, Zhang Y, *et al.* Synthesis and study on adsorption property of Congo red molecularly imprinted polymer nanospheres[J]. Environmental Science, 2015, **36**(7): 2564-
- [3] 张聪璐, 胡筱敏, 赵研, 等. 磁性壳聚糖衍生物对阴离子染料的吸附行为[J]. 环境科学, 2015, 36(1): 221-226.

  Zhang C L, Hu X M, Zhao Y, et al. Adsorption behavior of anionic dyes onto magnetic chitosan derivatives [J].

  Environmental Science, 2015, 36(1): 221-226.
- [4] Stawiński W, Węgrzyn A, Freitas O, et al. Simultaneous removal of dyes and metal cations using an acid, acid-base and base modified vermiculite as a sustainable and recyclable adsorbent [J]. Science of the Total Environment, 2017, 576: 398-408.
- [5] An A K, Guo J X, Jeong S, et al. High flux and antifouling properties of negatively charged membrane for dyeing wastewater treatment by membrane distillation[J]. Water Research, 2016, 103: 362-371.
- [ 6 ] Hadi P, Guo J X, Barford J, et al. Multilayer dye adsorption in activated carbons—facile approach to exploit vacant sites and interlayer charge Interaction [ J ]. Environmental Science & Technology, 2016, 50(10): 5041-5049.
- [7] Shao Y J, Ren B, Jiang H M, et al. Dual-porosity Mn<sub>2</sub>O<sub>3</sub> cubes for highly efficient dye adsorption [J]. Journal of Hazardous Materials, 2017, 333: 222-231.
- [8] 丁明,曾桓兴. 铁氧体工艺处理含重金属污水研究现状及展望[J]. 环境科学,1992,13(2):59-67.
  Ding M, Zeng H X. Progress and outlook on removing heavy metals from waste water by ferrite process[J]. Environmental Science, 1992,13(2):59-67.
- [9] Tu Y J, You C F, Chang C K, et al. Adsorption behavior of As( III) onto a copper ferrite generated from printed circuit board industry [J]. Chemical Engineering Journal, 2013, 225: 433-439.
- [10] 张立珠, 陈晓东, 马军, 等. 新生态 MnO<sub>2</sub> 强化混凝去除苯酚 的影响因素研究[J]. 环境科学, 2011, **32**(10): 2926-2930. Zhang L Z, Chen X D, Ma J, et al. Effects on phenol removal in the process of enhanced coagulation by manganese dioxide formed in situ [J]. Environmental Science, 2011, **32**(10): 2926-2930.
- [11] Lu X X, Huangfu X L, Zhang X, et al. Strong enhancement of trace mercury removal from aqueous solution with sodium thiosulfate by in situ formed Mn-(hydr) oxides [J]. Water Research, 2014, 65: 22-31.
- [12] Zhao F P, Repo E, Yin D L, et al. EDTA-cross-linked β-cyclodextrin; an environmentally friendly bifunctional adsorbent for simultaneous adsorption of metals and cationic dyes [J]. Environmental Science & Technology, 2015, 49 (17): 10570-10580.
- [13] Xu X Y, Huang F Z, Shao Y, et al. Improved magnetic and magnetoelectric properties in BaFe<sub>12</sub> O<sub>19</sub> nanostructures [ J ]. Physical Chemistry Chemical Physics, 2017, 19 (27): 18023-

- 18029
- [14] Tu Y J, Chang C K, You C F, et al. Treatment of complex heavy metal wastewater using a multi-staged ferrite process [J]. Journal of Hazardous Materials, 2012, 209-210: 379-384.
- [15] 常青, 江国栋, 胡梦璇, 等. 石墨烯基磁性复合材料吸附水中亚甲基蓝的研究[J]. 环境科学, 2014, **35**(5): 1804-1809.
  Chang Q, Jiang G D, Hu M X, et al. Adsorption of methylene
  - Chang Q, Jiang G D, Hu M X, et al. Adsorption of methylene blue from aqueous solution onto magnetic Fe<sub>3</sub>O<sub>4</sub>/Graphene oxide nanoparticles[J]. Environmental Science, 2014, **35**(5): 1804-1809.
- [16] Tang W S, Su Y, Li Q, et al. Superparamagnetic magnesium ferrite nanoadsorbent for effective arsenic (III, V) removal and easy magnetic separation[J]. Water Research. 2013, 47 (11): 3624-3634.
- [17] 刘伟,杨琦,李博,等. 磁性石墨烯吸附水中 Cr(VI)研究 [J]. 环境科学,2015,36(2):537-544.
  Liu W, Yang Q, Li B, et al. Adsorption of Cr(VI) on magnetic graphene from aqueous solution [J]. Environmental Science, 2015,36(2):537-544.
- [18] Zhuang Y, Yu F, Chen H, et al. Alginate/graphene double-network nanocomposite hydrogel beads with low-swelling, enhanced mechanical properties, and enhanced adsorption capacity[J]. Journal of Materials Chemistry A, 2016, 4(28): 10885-10892.
- [19] Iwunze M O. Determination of physico-chemical properties of Congo red in aqueous solution [J]. Physical Chemistry: An Indian Journal, 2010, 5(2): 84-89.
- [20] 孙德帅, 刘亚丽, 张晓东, 等. 铁有机骨架材料的快速合成及对阴离子染料的吸附性能[J]. 环境科学, 2016, 37(3): 1016-1022.
  Sun D S, Liu Y L, Zhang X D, et al. Rapid synthesis of metal organic framework and its adsorption properties on anonic dyes [J]. Environmental Science, 2016, 37(3): 1016-1022.
- [21] Wang L X, Li J C, Wang Y Q, et al. Preparation of nanocrystalline Fe<sub>3-x</sub>La<sub>x</sub>O<sub>4</sub> ferrite and their adsorption capability for Congo red[J]. Journal of Hazardous Materials, 2011, 196: 342, 340
- [22] Li D L, Yang Y G, Li C Z, et al. A mechanistic study on decontamination of methyl orange dyes from aqueous phase by mesoporous pulp waste and polyaniline [J]. Environmental Research, 2017, 154: 139-144.
- [23] Fu J W, Chen Z H, Wang M H, et al. Adsorption of methylene blue by a high-efficiency adsorbent (polydopamine microspheres): kinetics, isotherm, thermodynamics and mechanism analysis [J]. Chemical Engineering Journal, 2015, 259: 53-61.
- [24] Zhang X L, Feng M B, Qu R J, et al. Catalytic degradation of diethyl phthalate in aqueous solution by persulfate activated with nano-scaled magnetic CuFe<sub>2</sub>O<sub>4</sub>/MWCNTs [ J ]. Chemical Engineering Journal, 2016, 301: 1-11.
- [25] Guan Y H, Ma J, Ren Y M, et al. Efficient degradation of atrazine by magnetic porous copper ferrite catalyzed peroxymonosulfate oxidation via the formation of hydroxyl and sulfate radicals [J]. Water Research, 2013, 47 (14): 5431-5438.
- [26] Ding Y B, Zhu L H, Wang N, et al. Sulfate radicals induced degradation of tetrabromobisphenol A with nanoscaled magnetic CuFe<sub>2</sub>O<sub>4</sub> as a heterogeneous catalyst of peroxymonosulfate [J]. Applied Catalysis B: Environmental, 2013, 129: 153-162.

## **HUANJING KEXUE**

Environmental Science (monthly)

Vol. 39 No. 3 Mar. 15, 2018

## **CONTENTS**

Characterization and Variation of Organic Carbon (OC) and Elemental Carbon (EC) in PM <sub>2.5</sub> During the Winter in the Yangtze Ri	iver Delta Region, China ·····
Characterization and variation of organic carroin (00) and Editerial Carroin (20) in 1.12_5 butting its 4 miles in the Tangase In-	
Important Effect of Secondary Inorganic Salt Extinction on Visibility Impairment in the Northern Suburb of Nanjing	
Day-Night Differences and Source Apportionment of Inorganic Components of PM <sub>2.5</sub> During Summer-Winter in Changzhou City · · · · ·	······ LIU Jia-shu, GU Yuan, MA Shuai-shuai, et al. (980)
Characteristics of Elements in PM <sub>2.5</sub> and PM <sub>10</sub> in Road Dust Fall During Spring in Tianjin	······ WANG Shi-bao, JI Ya-qin, LI Shu-li, et al. (990)
Particle Size Distribution and Human Health Risk Assessment of Heavy Metals in Atmospheric Particles from Beijing and Xinxiang I	Ouring Summer
	···· ZHANG Xin, ZHAO Xiao-man, MENG Xue-jie, et al. (997)
$ Ecological \ and \ Health \ Risks \ of \ Trace \ Heavy \ Metals \ in \ Atmospheric \ PM_{2.5} \ Collected \ in \ Wuxiang \ Town, \ Shanxi \ Province $	···· GUO Zhao-xia, GENG Hong, ZHANG Jin-hong, et al. (1004)
Characteristics of Particulate and Inorganic Elements of Motor Vehicles Based on a Tunnel Environment	
A 2013-based Atmospheric Ammonia Emission Inventory and Its Characteristic of Spatial Distribution in Henan Province	
Emission Characteristics of Wind Erosion Dust from Topsoil of Urban Roadside-Tree Pool	····· LI Bei-bei, QIN Jian-ping, QI Li-rong, et al. (1031)
Particulate Component Emission Characteristic from a Diesel Bus with DOC and CDPF	LOU Di-ming, GENG Xiao-yu, SONG Bo, et al. (1040)
Water Quality in the Henan Intake Area of the South-to-North Water Diversion Project	
Spatio-Temporal Patterns and Environmental Risk of Endocrine Disrupting Chemicals in the Liuxi River	······ FAN Jing-jing, WANG Sai, TANG Jin-peng, et al. (1053)
Fate and Origin of Major Ions in River Water in the Lhasa River Basin, Tibet	······ ZHANG Qing-hua, SUN Ping-an, HE Shi-yi, et al. (1065)
Identification of Nitrate Sources and the Fate of Nitrate in Downstream Areas: A Case Study in the Taizi River Basin	
Sources, Distribution of Main Controlling Factors, and Potential Ecological Risk Assessment for Heavy Metals in the Surface Sedime	ent of Hainan Island North Bay, South China
ZEI	
Characteristics of Heavy Metals Pollution of Farmland and the Leaching Effect of Rainfall in Tianjin	
Seasonal Difference in Water Quality Between Lake and Inflow/Outflow Rivers of Lake Taihu, China	
Characteristics of Nitrogen Release at the Sediment-Water Interface in the Typical Tributaries of the Three Gorges Reservoir During	the Sensitive Period in Spring
71 0 0	
Spatial Distributions of Transferable Nitrogen Forms and Influencing Factors in Sediments from Inflow Rivers in Different Lake Basin	
Effects of Hydrological and Meteorological Conditions on Diatom Proliferation in Reservoirs	
Vertical Distribution of Fungal Community Composition and Water Quality During the Deep Reservoir Thermal Stratification S	
Community Structure and Influencing Factors of Bacterioplankton in Spring in Zhushan Bay, Lake Taihu	XUE Yin-gang, LIU Fei, SUN Meng, et al. (1151)
Characteristics of Sediment Oxygen Demand in a Drinking Water Reservoir	SU Lu, HUANG Ting-lin, LI Nan, et al. (1159)
Effects of Wastewater Nitrogen Concentrations and NH <sub>4</sub> <sup>+</sup> /NO <sub>3</sub> <sup>-</sup> on Nitrogen Removal Ability and the Nitrogen Component of Myrioph	nyllum aquaticum (Vell.) Verdc ·····
4 3 0 7 0 1 7 1	·· MA Yong-fei, YANG Xiao-zhen, ZHAO Xiao-hu, et al. (1167)
Effect of Nutrient Loadings on the Regulation of Water Nitrogen and Phosphorus by Vallisneria natans and Its Photosynthetic Fluores	cence Characteristics ·····
Enter of Fundamental Indication of Water Militager and Thosphoras by Parison of Water Malay and 15 Thorough Indication of Water Malay and 15 Thorough Indication of Water Malay and 15 Thorough Indication of Water Malay and Indication of Water Mala	··· ZHOU Yi-wen, XU Xiao-guang, HAN Rui-ming, et al. (1180)
Removal of Organic Matter from Water by Chemical Preoxidation Coupled with Biogenic Manganese Oxidation	·· JIAN Zhi-yu, CHANG Yang-yang, WANG Li-xin, et al. (1188)
Treating Simulated Dye Wastewater by an In Situ Copper Ferrite Process	······· HAN Zhi-yong, HAN Kun, HAO Hao-tian, et al. (1195)
Experiment to Enhance Catalytic Activity of α-FeOOH in Heterogeneous UV-Fenton System by Addition of Oxalate ····································	
Fabrication of a Biomass-Based Hydrous Zirconium Oxide Nanocomposite for Advanced Phosphate Removal	······ QIU Hui, QIN Zhi-feng, LIU Feng-ling, et al. (1212)
Characteristic of Nitrate Adsorption in Aqueous Solution by Iron and Manganese Oxide/Biochar Composites	ZHENG Xiao-qing, WEI An-lei, ZHANG Yi-xuan, et al. (1220)
Preparation of PAAm/HACC Semi-Interpenetrate Network Hydrogel and Its Adsorption Properties for Humic Acid from Aqueous Solu	tion LIU Ze-jun, ZHOU Shao-qi, MA Fu-zhen (1233)
Groundwater Arsenic and Silicate Adsorption on TiO2 and the Regeneration of TiO2	MA Wen-jing, YAN Li, ZHANG Jian-feng ( 1241 )
Removal Efficiency and Mechanism of Removal by Humic Acid of the Integrated Floc-ultrafiltration Process	LI Wen-jiang, YU Li-fang, MIAO Rui, et al. (1248)
Emission Inventory of Greenhouse Gas from Urban Wastewater Treatment Plants and Its Temporal and Spatial Distribution in China	······· YAN Xu, QIU De-zhi, GUO Dong-li, et al. (1256)
Start-up and Operation of Biofilter Coupled Nitrification and CANON for the Removal of Iron, Manganese and Ammonia Nitrogen · · ·	······ LI Dong, CAO Rui-hua, YANG Hang, et al. (1264)
Analysis of CANON Process Start-up with Fiber Carrier	GU Cheng-wei, CHEN Fang-min, LI Xiang, et al. (1272)
Characteristics of Biofilm During the Transition Process of Complete Nitrification and Partial Nitrification	ZHAO Qing, BIAN Wei, LI Jun, et al. (1278)
Effect of Intermediate-Setting Aeration on the CANON Granular Sludge Process in the AUSB Reactor	CHENG Shuo, LI Dong, ZHANG Jie, et al. (1286)
Effect of Organic Carbon Source on Start-up and Operation of the CANON Granular Sludge Process · · · · · · · · · · · · · · · · · ·	LI Dong, WANG Yan-ju, LÜ Yu-feng, et al. (1294)
Start-Up and Regional Characteristics of a Pilot-scale Integrated PN-ANAMMOX Reactor	ZHOU Zheng, WANG Fan, LIN Xing, et al. (1301)
Effect of NO - N Recycling Ratio on Denitrifying Phosphorus Removal Efficiency in the ABR-MBR Combined Process	LÜ Liang, YOU Wen, ZHANG Min, et al. (1309)
Effects of Magnetic Fe <sub>3</sub> O <sub>4</sub> Nanoparticles on the Characteristics of Anaerobic Granular Sludge and Its Interior Microbial Community	
Characterization Composition of Soluble Microbial Products in an Aerobic Granular Sludge System	YANG Dan, LIU Dong-fang, DU Li-giong, et al. (1325)
Influence of Ciprofloxacin on the Microbial Community and Antibiotics Resistance Genes in a Membrane Bioreactor	
Analysis of Low C/N Wastewater Treatment and Structure by the CEM-UF Combined Membrane-Nitrification/Denitrification System	
	XING Jin-liang, ZHANG Yan, CHEN Chang-ming, et al. (1342)
Effects of Phosphorus on the Activity and Bacterial Community in Mixotrophic Denitrification Sludge	
Acclimatization and Community Structure Analysis of the Microbial Consortium in Nitrate-Dependent Anaerobic Methane Oxidation	1, , ,
Diffusion of Microorganism and Main Pathogenic Bacteria During Municipal Treated Wastewater Discharged into Sea	
Oxytetracycline Wastewater Treatment in Microbial Fuel Cells and the Analysis of Microbial Communities	
Spatial and Temporal Variability of Soil C-to-N Ratio of Yugan County and Its Influencing Factors in the Past 30 Years	
Spatial Heterogeneity of Soil Carbon and its Fractions in the Wolfberry Field of Zhongning County	
Response of Soil Enzyme Activities and Their Relationships with Physicochemical Properties to Different Aged Coastal Reclamation A	Areas, Eastern China ·····
Response of Soil Enzyme Activities and Their Relationships with Physicochemical Properties to Different Aged Coastal Reclamation	Areas, Eastern China
	············ XIE Xue-feng, PU Li-jie, WANG Qi-qi, et al. (1404)
Distribution. Sources, and Ecological Risk Assessment of Polycyclic Aromatic Hydrocarbons (PAHs) in Soils of the Central and Ea	
Distribution, Sources, and Ecological Risk Assessment of Polycyclic Aromatic Hydrocarbons (PAHs) in Soils of the Central and Ea	XIE Xue-feng, PU Li-jie, WANG Qi-qi, et al. (1404) stern Areas of the Qinghai-Tibetan Plateau
Distribution, Sources, and Ecological Risk Assessment of Polycyclic Aromatic Hydrocarbons (PAHs) in Soils of the Central and Ea  Source Apportionment of Heavy Metals in Farmland Soils Around Mining Area Based on UNMIX Model	XIE Xue-feng, PU Li-jie, WANG Qi-qi, et al. (1404) stern Areas of the Qinghai-Tibetan Plateau ZHOU Wen-wen, LI Jun, HU Jian, et al. (1413) LU Xin, HU Wen-you, HUANG Biao, et al. (1421)
Distribution, Sources, and Ecological Risk Assessment of Polycyclic Aromatic Hydrocarbons (PAHs) in Soils of the Central and Ea	XIE Xue-feng, PU Li-jie, WANG Qi-qi, et al. (1404) stern Areas of the Qinghai-Tibetan Plateau ZHOU Wen-wen, LI Jun, HU Jian, et al. (1413) LU Xin, HU Wen-you, HUANG Biao, et al. (1421) FEI Yang, YAN Xiu-lan, LI Yong-hua (1430)